Structure, phase transitions and molecular motions in ferroelastic $(C_4H_8NH_2)SbCl_6 \cdot (C_4H_8NH_2)Cl$

2002 J. Phys.: Condens. Matter 14 3129

(http://iopscience.iop.org/0953-8984/14/12/305)

INSTITUTE OF PHYSICS PUBLISHING JOURNAL OF PHYSICS: CONDENSED MATTER

J. Phys.: Condens. Matter **14** (2002) 3129–3142 PII: S0953-8984(02)28092-3

Structure, phase transitions and molecular motions in ferroelastic $(C_4H_8NH_2)SbCl_6\cdot(C_4H_8NH_2)Cl$

B Bednarska-Bolek[1], R Jakubas[1,5], W Medycki[2], D Nowak[3] and J Zaleski[4]

[1] Faculty of Chemistry, University of Wrocław, Joliot–Curie 14, 50–383 Wrocław, Poland
[2] Institute of Molecular Physics, PAS, Smoluchowskiego 17, 60-179 Poznań, Poland
[3] Institute of Physics, UAM, Umultowska 85, 61-614 Poznań, Poland
[4] Institute of Chemistry, University of Opole, Oleska 48, 45-951 Opole, Poland

E-mail: rj@wchuwr.chem.uni.wroc.pl

Received 20 August 2001, in final form 4 December 2001
Published 15 March 2002
Online at stacks.iop.org/JPhysCM/14/3129

Abstract

The crystal structure at 293 K of the new pyrrolidinium chloroantimonate (V) analogue, $(C_4H_8NH_2)SbCl_6\cdot(C_4H_8NH_2)Cl$, has been determined by x-ray diffraction as monoclinic, space group $P2_1/c$, $Z = 8$. The crystal is built up of isolated $SbCl_6^-$ anions, two types of inequivalent pyrrolidinium cation and isolated Cl^- ions. It undergoes five solid–solid phase transitions: at 351/374 K of first-order type (cooling/heating, respectively), at 356 and 152 K second order and at 135/141 and 105/134 K first order, detected by differential scanning calorimetry, dilatometric and dielectric measurements. The ferroelastic domain structure appears between 152 and 135 K. The proton nuclear magnetic resonance second moment and spin–lattice relaxation time of polycrystalline samples were studied over the temperature range 27–410 K. The order–disorder mechanism of the phase transitions at 105 and 374 K connected with the reorientational motion of the pyrrolidinium cations has been confirmed.

1. Introduction

Chloroantimonates (V) of the general formula $RSbCl_6$ (R denotes an organoammonium cation) form a new class of ferroic crystals. Several salts belonging to this family exhibit ferroelastic properties, for example $[P(CH_3)_4]SbCl_6$ [1], $[C(NH_2)_3]SbCl_6$ [2], $[(C_2H_5)_3NH]SbCl_6$ [3] and $[C_5H_{10}NH_2]SbCl_6$ [4]. The structure of these salts consists of isolated $SbCl_6$ octahedra connected by weak N–H$\cdots$Cl hydrogen bonds to the organic cations. Closely related to this family is a second piperidinium analogue, namely $(C_5H_{10}NH_2)SbCl_6\cdot(C_5H_{10}NH_2)Cl$, exhibiting ferroelastic properties [5]. In comparison with the $RSbCl_6$ class of crystals the $RSbCl_6\cdot RCl$ subgroup is characterized by a more complex structure. In the crystal lattice

[5] Author to whom any correspondence should be addressed.

of $(C_5H_{10}NH_2)SbCl_6{\cdot}(C_5H_{10}NH_2)Cl$, apart from isolated $SbCl_6^-$ anions and $(C_5H_{10}NH_2)^+$ cations, there appear isolated Cl^- ions. Compounds with the $RSbCl_6{\cdot}RCl$ and $RSbCl_6$ stoichiometry are characterized by quite a complex sequence of phase transitions (PTs). In their high-temperature (paraelastic) phases both the $SbCl_6^-$ anions and organic cations are performing isotropic motion. In general, the paraelastic phases in chloroantimonates (V) resemble the ionic plastic ones. Most of the PTs in the above-mentioned chloroantimonate (V) salts exhibit an order–disorder character and are mainly due to changes in the disorder of the organic cations. In search of new ferroic crystals, we decided to incorporate into the crystal lattice of the chloroantimonate (V) salts the cyclic organoammonium cation pyrrolidinium, $(C_4H_8NH_2)^+$.

In this paper we report x-ray, differential scanning calorimetry (DSC), dilatometry and dielectric studies of a new ferroic compound, pyrrolidinium chloroantimonate (V), $(C_4H_8NH_2)SbCl_6{\cdot}(C_4H_8NH_2)Cl$ (abbreviated as PRCA). Optical observations of the domain structure are reported. ^{1}H NMR (nuclear magnetic resonance) studies are undertaken to explain the role of the pyrrolidinium cations in the mechanism of the PTs in the title crystal. Since this is only the second example of chloroantimonates (V) with $RSbCl_6{\cdot}Cl$ stoichiometry it seemed interesting to determine how the structure of the anionic sublattice influences the sequence of PTs and ferroic properties.

2. Experimental details

$(C_4H_8NH_2)SbCl_6{\cdot}(C_4H_8NH_2)Cl$ was prepared by the reaction of $SbCl_5$ and $(C_4H_8NH_2)Cl$ (molar ratio 2:1) in concentrated HCl. The resulting white solid was recrystallized twice from an ethanol solution. Single crystals of the title compound were grown from the solution at constant room temperature (RT).

DSC measurements were carried out using a Perkin-Elmer DSC-7 calorimeter with a scanning rate 10 K min^{-1} on cooling/heating.

Linear thermal expansion was measured using a thermomechanical analyser—Perkin-Elmer TMA-7. The samples used in the measurements were prepared in the form of thin plates ($4 \times 4 \times 1$ mm^3). The accuracy of thermal expansion determination was about 3%.

The complex electric permittivity, ε^*, for a single crystal of PRCA was measured by an HP 4285A precision *LCR* meter over the frequency range 75 Hz–20 MHz. The measurements were performed in the temperature range 95–380 K. The temperature of the specimen was varied continuously with the rate of 0.1 K min^{-1} in the vicinity of the PT points and 0.5 K min^{-1} elsewhere. Samples for dielectric measurements were typically of size $4 \times 3 \times 1$ mm^3. The plates were silver painted. The accuracy of the measured electric permittivity value was about 5%.

NMR measurements were performed on a Bruker SXP 4–100 spectrometer working at the frequency of 24.7 and 90 MHz. The temperature of the sample was automatically stabilized by a Leybold temperature controller or by a Bruker BS 100/700 liquid nitrogen controller. The T_1 relaxation times were determined by using the $\pi{-}\tau{-}\pi/2$ sequence of pulses for times shorter than 1 s and by the saturation method for longer times. The second moment of NMR lines for protons was found on the basis of analysis of the solid echo shape.

Data for the structure determination were collected on a KUMA KM4 κ-axis diffractometer with graphite monochromated Mo Kα radiation, $\lambda = 0.710\,73$ Å. The crystal data and experimental conditions are listed in table 1. The lattice parameters were refined from setting angles of 25 reflections in the $13^\circ < 2\theta < 24^\circ$ range. Two control reflections measured after an interval of 50 show no significant intensity variations. The structure was solved by the Patterson method and refined by a full-matrix least-squares method. The calculated difference Fourier

Table 1. Crystal data and structure refinement for PRCA.

Empirical formula	C4 H10 Cl3.50 N Sb0.50
Formula weight	257.08
Temperature	293(2) K
Wavelength	0.710 73 Å
Crystal system, space group	Monoclinic, $P2_1/c$
Unit cell dimensions	$a = 10.363(2)$ Å
	$b = 21.570(4)$ Å
	$c = 9.848(2)$ Å
	$\beta = 118.07(3)^\circ$
Volume	1942.4(7) Å^3
Z, calculated density	8, 1.758 mg m^{-3}
Absorption coefficient	2.370 mm^{-1}
$F(000)$	1008
θ range for data collection	2.23°–25.05°
Limiting indices	$-10 \leqslant h \leqslant 11, 0 \leqslant k \leqslant 25, -10 \leqslant l \leqslant 0$
Reflections collected/unique	3285/3097 (R(int) = 0.0287)
Refinement method	Full matrix least squares on F^2
Data/restraints/parameters	3097/12/173
Goodness of fit on F^2	1.117
Final R indices ($I > 2\sigma(I)$)	$R_1 = 0.0405$, w$R_2 = 0.1135$
R indices (all data)	$R_1 = 0.0539$, w$R_2 = 0.1198$
Largest diff. peak and hole	0.716 and −0.435 e Å^{-3}

maps revealed a large disorder in the C atom of one of two independent cations. Parameters of non-hydrogen atoms were refined using anisotropic temperature factors. All hydrogen atoms were included using standard geometric criteria. Hydrogen atoms of methylene groups were constrained to distances of 0.96 Å, the H atoms of the amine group to 0.90 Å. The positions of hydrogen atoms were refined using a riding model. KUMA software was used in data collection, cell refinement and data reduction processes [6]. The SHELX-97 program [7] was used for structure solution and refinement. The structure drawings were prepared using the SHELXTL program [8]. Final atomic coordinates and equivalent isotropic displacement parameters for non-H atoms are shown in table 2. A list of calculated and observed structure factors may be obtained from the authors on request.

3. Results

3.1. X-ray data

The PRCA compound at RT crystallizes in the monoclinic $P2_1/c$ space group. The independent part of the unit cell consists of one $SbCl_6^-$ octahedron, one isolated chlorine ion and two symmetry-independent pyrrolidinium cations (labelled N(1) and N(6) in the text). The Sb–Cl bond lengths are in a range 2.336(2)–2.366(2) Å. The Cl–Sb–Cl bond angles '*cis*' with respect to each other fall in the range 89.3(1)°–90.9(1)°, whereas those '*trans*' are between 178.8(1)° and 179(2)°. They are only slightly distorted, especially in comparison with differences in bond lengths and angles found in the Sb (III) salts [9, 10]. The selected bond lengths, angles and hydrogen bond geometry are given in table 3.

The C(3) atom opposite the N atom of the ring (cation N(1)) has a large displacement amplitude perpendicular to the plane of the ring. For this type of cation the disordering model is proposed. The disorder is realized by splitting of the C(3) atom between two sites with half

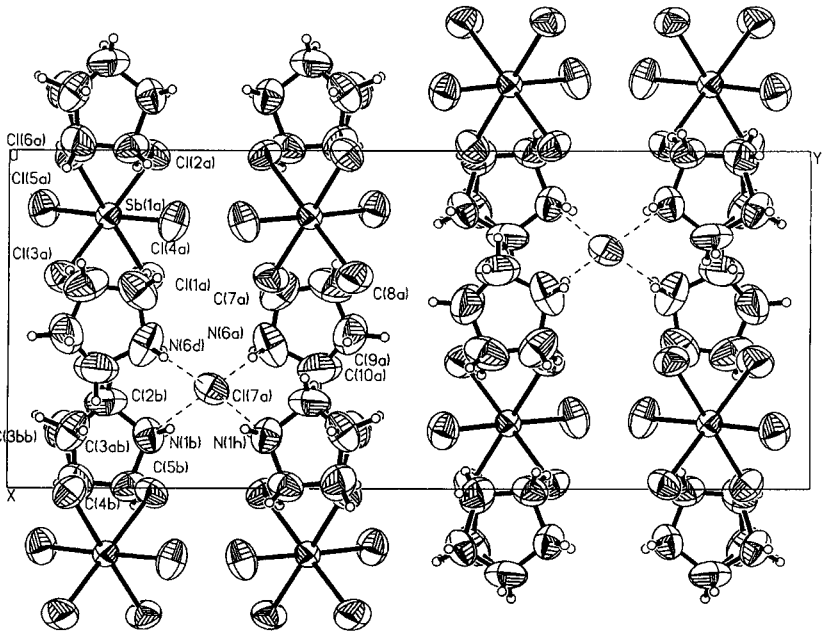

Figure 1. Projection of the crystal lattice of $(C_4H_8NH_2)SbCl_6 \cdot (C_4H_8NH_2)Cl$ onto the *a*–*b* plane at 293 K.

Table 2. Atomic coordinates ($\times 10^4$) and equivalent isotropic displacement parameters ($Å^2 \times 10^3$) for PRCA. (U(eq) is defined as one-third of the trace of the orthogonalized U_{ij} tensor.)

	x	*y*	*z*	*U*(eq)
Sb(1)	1957(1)	1246(1)	2015(1)	51(1)
Cl(1)	3781(2)	1721(1)	1574(2)	81(1)
Cl(2)	143(2)	1805(1)	−81(2)	77(1)
Cl(3)	3767(2)	681(1)	4083(2)	97(1)
Cl(4)	2125(3)	2062(1)	3676(2)	90(1)
Cl(5)	1734(2)	437(1)	341(2)	91(1)
Cl(6)	127(2)	783(1)	2468(2)	82(1)
Cl(7)	−2948(2)	2549(1)	−3276(2)	78(1)
N(1)	−1572(7)	1761(3)	−5004(7)	82(2)
C(2)	−2557(10)	1231(5)	−5407(14)	129(4)
C(3A)	−1700(2)	815(10)	−4170(3)	105(6)
C(3B)	−1760(19)	669(8)	−5160(2)	84(5)
C(4)	−191(10)	865(4)	−3885(11)	105(3)
C(5)	−58(8)	1522(4)	−4098(9)	81(2)
N(6)	5763(10)	3278(3)	3534(7)	100(2)
C(7)	4179(11)	3385(5)	2915(10)	106(3)
C(8)	4005(11)	4027(6)	3106(12)	114(3)
C(9)	5446(12)	4272(5)	4056(16)	141(4)
C(10)	6447(10)	3892(6)	3835(15)	129(4)

occupancy. During the solution of the structure we have to decide which atoms are nitrogen and which carbons. This has been done arbitrarily based on distances between the respective atoms and chlorines. For the second cation (N(6)), especially the C(9) and C(10) atoms have high anisotropic temperature coefficients (see table 2). This clearly indicates disorder resulting from

Table 3. Selected bond lengths (Å) and angles (°) and hydrogen bond distances and angles for PRCA.

Anion	
Sb(1)–Cl(1)	2.363(2)
Sb(1)–Cl(2)	2.366(2)
Sb(1)–Cl(3)	2.358(2)
Sb(1)–Cl(4)	2.353(2)
Sb(1)–Cl(5)	2.336(2)
Sb(1)–Cl(6)	2.364(2)
Cl(5)–Sb(1)–Cl(4)	178.78(1)
Cl(5)–Sb(1)–Cl(3)	89.8(1)
Cl(4)–Sb(1)–Cl(3)	91.0(1)
Cl(5)–Sb(1)–Cl(1)	90.9(1)
Cl(4)–Sb(1)–Cl(1)	90.0(1)
Cl(3)–Sb(1)–Cl(1)	90.2(1)
Cl(5)–Sb(1)–Cl(6)	89.8(1)
Cl(4)–Sb(1)–Cl(6)	89.3(1)
Cl(3)–Sb(1)–Cl(6)	90.1(1)
Cl(1)–Sb(1)–Cl(6)	179.2(1)
Cl(5)–Sb(1)–Cl(2)	89.5(1)
Cl(4)–Sb(1)–Cl(2)	89.7(1)
Cl(3)–Sb(1)–Cl(2)	179.3(1)
Cl(1)–Sb(1)–Cl(2)	89.7(1)
Cl(6)–Sb(1)–Cl(2)	90.1(1)

Hydrogen bonds

D–H···A	d(D···H)	d(H···A)	d(D···A)	<(DHA)
N(1)–H(1A)···Cl7[a]	0.90	2.386	3.210(2)	156
N(1)–H(1B)···Cl7	0.90	2.310	3.178(2)	163
N(6)–H(6A)···Cl7[b]	0.90	2.292	3.191(2)	177
N(1)–H(6B)···Cl7[c]	0.90	2.351	3.223(2)	163

Symmetry transformations used to generate equivalent atoms:
[a] $x, 0.5 - y, z - 0.5$
[b] $x + 1, y, z + 1$
[c] $x + 1, 0.5 - y, z + 0.5$.

some ring motion. The crystal packing of PRCA is presented in figure 1. Both symmetry-independent pyrrolidinium cations are connected by weak N–H···Cl hydrogen bonds with isolated chlorine atoms (see table 3).

3.2. Differential scanning calorimetry (DSC) and dilatometric measurements

The DSC curves for the PRCA crystal over the temperature range 95–410 K are presented in figure 2. The phase situation disclosed in this crystal seems to be quite complex and depends on the thermal history of the sample. During the first cooling run (scan 1) performed between RT and 110 K, PRCA revealed two thermal anomalies, corresponding to structural PTs at 152 K of second-order type and at 135 K of first order, which are readily reversible. During the heating scan (scan 2) these PTs appears at 152 and 141 K, respectively. If the sample is cooled down again to 95 K (scan 3), apart from the PTs at 152 and 135 K, a strong heat anomaly connected with the first-order PT at 105 K is visible. The fourth scan, performed between 95 and 400 K, in the low-temperature region shows unexpectedly only one strong thermal anomaly at 134 K, which is undoubtedly attributable to the reversible lowest-temperature PT (105 K). Since this PT is characterized by a very large temperature hysteresis, it may overlap with the PT visible at 135 K during the cooling scan. Further heating of the PRCA sample up to 400 K shows that it undergoes two PTs: at 356 K of second-order and at 374 K of first-order type. During the last cooling cycle (scan 5), over the high-temperature region, only one strong heat anomaly at 351 K is visible, indicating the reversibility of the highest-temperature PT. Because of the

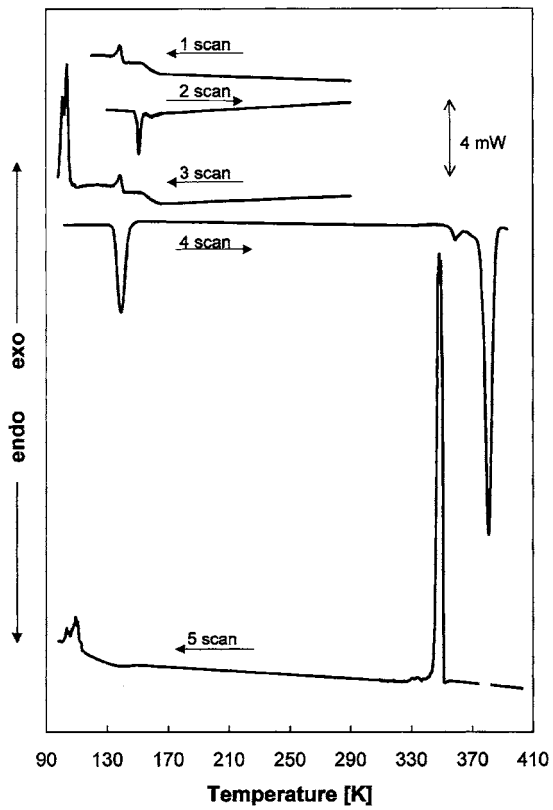

Figure 2. DSC curves of the PRCA crystal for several scans between 95 and 410 K (scanning rate 10 K min^{-1}, sample mass 17.47 mg).

Table 4. Thermodynamic parameters of the structural PTs in PRCA (T_c, T_h—temperature on cooling and heating, respectively).

T_c	T_h	ΔH (kJ mol^{-1})	ΔS (J mol^{-1} K^{-1})	Order
351	374	10.028	28.5 (R ln 30.8)	First
—	356			Second
152	152			Second
135	141	0.103	0.78 (R ln 1.1)	First
105	134	1.074	10.2 (R ln 3.4)	First

large temperature hysteresis ($\Delta T = 23$ K), it overlaps with the possible positions of heat anomaly corresponding to PT at 356 K. On further cooling of the crystal (see scan 5) in the low-temperature region, instead of the expected three PTs only the lowest-temperature PT at about 105 K is now recorded. Results of the calorimetric studies of PRCA are collected in table 4.

The overall behaviour of the linear thermal expansion of the PRCA single crystal along three crystallographic axes during cooling and heating scans over the low- and the high-temperature regions is shown in figure 3 (the directions presented correspond to those taken for the monoclinic RT phase; the c^* direction makes an angle of about 18° with the c axis). Above RT the continuous PT at 356 K is hardly visible in thermal dilation, whereas the 374 K

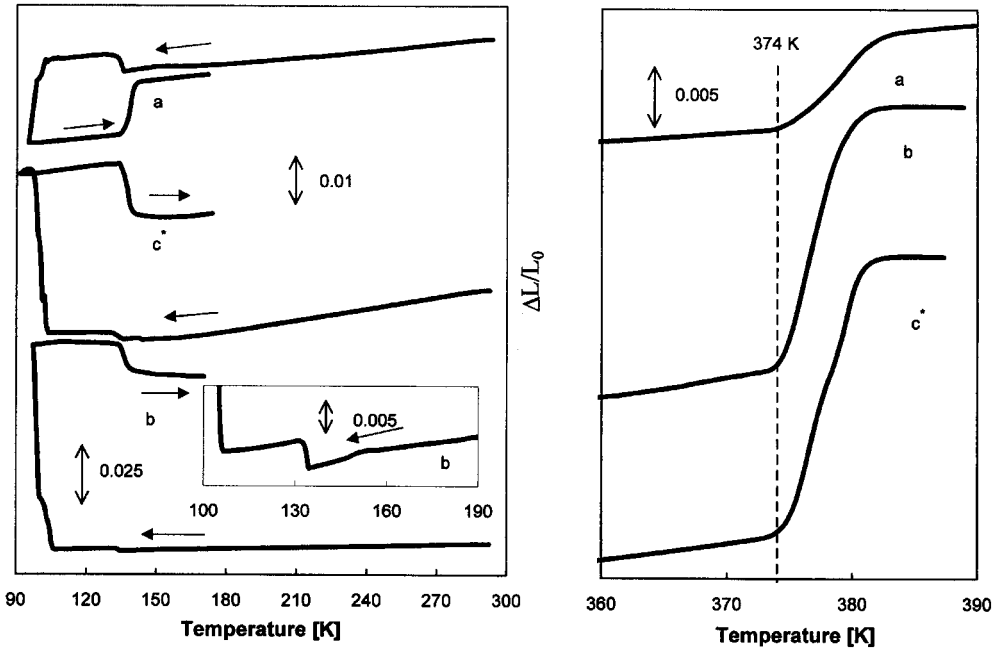

Figure 3. Temperature dependence of the linear thermal expansion along the a, b and c^* axes during cooling and heating runs over the low- (left-hand side) and high-temperature (right-hand side) regions during heating.

PT is accompanied by a distinct expansion of the sample along all the directions. In the low-temperature region (see figure 3), three PTs are clearly visible during the cooling cycle. The second-order PT at 152 K is accompanied by a subtle change in the slope of the $\Delta L/L_0$(T) curve (for the a and b directions). The PT at 135 K is accompanied by comparable anomalies in dilations along all the directions. In turn, the lowest-temperature PT at 105 K reveals a drastic expansion of the sample along the c^* and b directions and a small compression for the a axis. Then, during the heating cycle the directions of these changes in the vicinity of the 134 K PT are reversible; however, the $\Delta L/L_0$ values of these changes are several times smaller. It should be added that the 105 K PT yields to a complete deformation of the single-crystal sample. One can also state that the character of the PTs and the phase situation disclosed by means of the dilatometric measurements for the PRCA crystal is well consistent with those found by the DSC studies.

3.3. Dielectric studies

The temperature dependence of the real part of the complex electric permittivity, ε'_b, measured between 75 kHz and 30 MHz on cooling is shown in figure 4. From among four PTs disclosed by the DSC and dilatometric studies (during cooling cycles) only three are active in the dielectric measurements. The most interesting dielectric response is seen around the 351 K PT. This transition is accompanied by a drastic jump in the ε'_b value. The shape of this anomaly is typical of the compounds exhibiting a so-called 'rotator phase'. The divergence in the electric permittivity value around the PT at 351 K does not exhibit the feature of the dielectric relaxation process. The dielectric increment ($\Delta\varepsilon_b$) close to 351 K PT is quite large in comparison with those visible in the low-temperature region at 135 and 105 K. The dielectric anomaly at 351 K

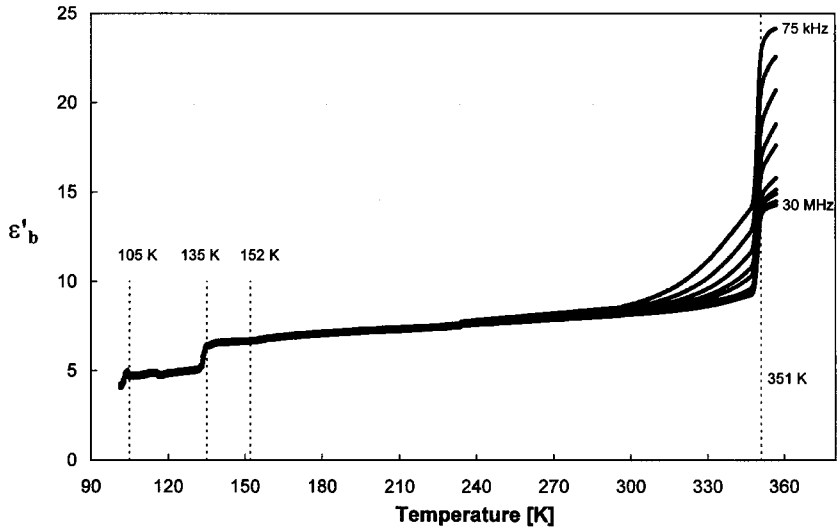

Figure 4. Temperature dependence of the real part of the complex electric permittivity, ε^*, measured along the b axis over the frequencies 75 kHz–30 MHz on cooling. The broken lines show the transition temperatures determined by DSC on cooling.

may be connected with the freezing of rotational motion of the pyrrolidinium rings. Such a type of motion seems to lead to an essential change in the resultant dipole moment of the unit cell.

3.4. ^1H NMR studies

The NMR measurements were carried out on cooling in the low-temperature region, from RT to 27 K, whereas on heating above RT. The temperature dependence of the second moment of the proton resonance lines, M_2, of PRCA is shown in figure 5. It is seen that between 27 and 105 K the second moment has a plateau of about 9×10^{-8} T^2. Above 105 K the M_2 value drops to about 8×10^{-8} T^2 and then from 152 K M_2 decreases continuously, reaching 5×10^{-8} T^2 at 220 K. It remains constant from 220 to 374 K and above the PT at 374 K a rapid fall in the M_2 value to 3.6×10^{-8} T^2 is observed. The plateau of 3.6×10^{-8} T^2 is maintained to at least 410 K. It should be underlined that the full isotropic motion of the pyrrolidinium cation is not reached up to 410 K.

The basic equation for the dipolar second moment, M_2, of a dipolar NMR line was derived by van Vleck [11]:

$$M_2^{\text{rigid}} = \frac{3}{5} I(I+1)\gamma^2\hbar^2 \frac{1}{N} \sum_{i=1}^{N} \sum_{j=1}^{N} R_{ij}^{-6} \tag{1}$$

where N is the number of protons in the unit cell. The value of M_2^{rigid} calculated from the crystal structure of PRCA (this paper) appeared to be quite large, being about 37.9×10^{-8} T^2. In the presence of motions for which $\tau_c \ll 1/(2\pi\delta\nu)$, where $\delta\nu$ is the line width in a frequency scale, the second moment is reduced by about ΔM_2. The reduced value of second moment is M_2^{motion}. It is known that the reduced value of the second moment due to the motion is described by the equation [12]

$$\Delta M_2(\tau_c) = \tfrac{3}{4} M_2^{\text{rigid}}. \tag{2}$$

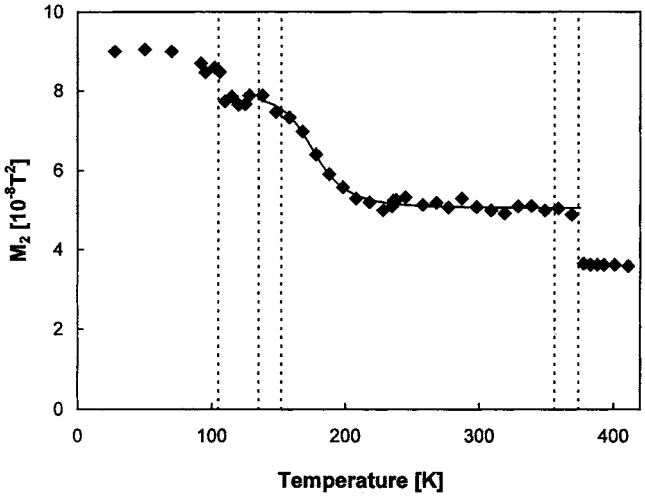

Figure 5. Temperature dependence of the second moment of the proton NMR lines (M_2) for PRCA. The broken lines show the transition temperatures determined by DSC.

The reduction takes place below 27 K, probably close to liquid helium temperature. The nature and dynamical parameters of the above motion are not clear. The tunnelling of the pyrrolidinium cations should be taken into account to explain the discussed effect. It is interesting to note that the observed M_2^{motion} equal to 9×10^{-8} T^2 satisfies this equation excellently. Above 135 K, the second-moment value decreases from about 8 to 5×10^{-8} T^2. Analysis of the temperature dependence of M_2 can be performed on the basis of the BPP formula:

$$M_2 = M_2^{\text{II}} + (M_2^{\text{I}} - M_2^{\text{II}}) \frac{2}{\pi} \tan^{-1}(\gamma \sqrt{M_2} \tau_c) \tag{3}$$

where $\tau_c = \tau_0 \exp(E_a/RT)$, M_2^{I} and M_2^{II} are the second-moment values before and after the onset of a given motion, respectively. The reduction of the second moment is the result of the fit with equation (3) with the activation energy of 3.7 kcal mol^{-1} and the correlation time of 6.2×10^{-11} s.

Figure 6 shows the plot of spin–lattice relaxation time (T_1) versus $1000/T$ at the two Larmor frequencies 24.7 (circles) and 90 MHz (triangles). In all existing phases the non-exponential recovery of ^{1}H magnetization has been observed. Such a recovery curve could be separated into two relaxation times, T_1^S and T_1^L ($T_1^S < T_1^L$), according to the equation

$$(M_0 - M_z(\tau))/M_0 = A_S \exp(-\tau/T_1^S) + A_L \exp(-\tau/T_1^L) \tag{4}$$

where M_0 and $M_z(\tau)$ are components of magnetization at thermal equilibrium and at time τ after the saturation sequence, respectively. A_S and A_L are constants and $A_S + A_L = 1$. In the whole studied temperature range the mutual relation between the two observed components seems to be in the 2:1 proportion. Currently, there is no satisfactory interpretation of this fact. A similar effect has been observed in the case of the $(C_4H_8NH_2)PF_6$ crystal [13]. Near the PT at 105 K in PRCA the longer component of the relaxation time, T_1^L, changes rapidly but the short one, T_1^S, does not. In the case of the PT at 135 K the situation is inverted. No changes are noticeable at 152 K. Close to the PT at 374 K the magnitude of the short component T_1^S is growing. The two relaxation time minima have been detected for the longer components at 24.7 and 90 MHz around the 135 K PT. We attempted to approximate the T_1 data with the

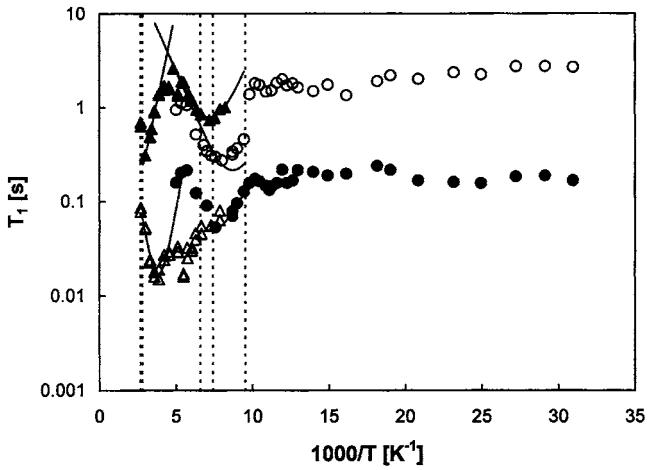

Figure 6. Proton spin–lattice relaxation times T_1 versus 1000 K^{-1} for 24.7 MHz (○—long component T_1^l, ●—short component T_1^s) and 90 MHz (▲—T_1^l, Δ—T_1^s). The broken lines show the transition temperatures determined by DSC.

Table 5. Activation energies (E_a), correlation times (τ_{co}) and motional constants (C) evaluated for pyrrolidinium cations.

ω_0 (MHz)	T_{min} (K)	Component	C (s^{-2})	E_a (kcal mol^{-1})	τ_{co} (s)
24.7	115	Long	4.2×10^8	1.72	4.1×10^{-12}
90	139	Long	4.2×10^8	1.72	4.1×10^{-12}
24.7	137	Short		1.55	
90	261	Short	2.3×10^{10}	4.1	4.1×10^{-13}
90	374	Long		3.6	

BPP-type equation [14]:

$$\frac{1}{T_1} = C\left(\frac{\tau_c}{1+\omega_0^2\tau_c^2} + \frac{4\tau_c}{1+4\omega_0^2\tau_c^2}\right) \tag{5}$$

where C denotes the motional constant, τ_c the correlation time and ω_0 the Larmor frequency. The temperature dependence of correlation times in the temperature range of this fit is described by the Arrhenius law $\tau_c = \tau_{co}\exp(E_a/RT)$. The obtained parameters are given in table 5. The visible discrepancy between the measured T_1 relaxation time and calculated theoretical line (see T_1^L for 24.7 MHz in figure 6) may be attributed to the possible influence of an additional relaxation process of protons via quadrupolar nuclei of ^{35}Cl.

Between the temperatures of 105 and 135 K the activation energy of 1.55 kcal mol^{-1} is derived. Next, from the slope of the short component the activation energy of 4.1 kcal mol^{-1} is found and the analogous activation energy from the long component was estimated to be 3.6 kcal mol^{-1} (see the fitted curve for both components of the 90 MHz Larmor frequency before the PT at 374 K). The activation energies found point to two different motional states of the pyrrolidinium cations in PRCA. The following kinds of motion of the cations may be considered in the studied temperature region:

(1) rigid sublattice cation,
(2) a pucking motion of the pyrrolidinium cation between twisted and envelope conformations,

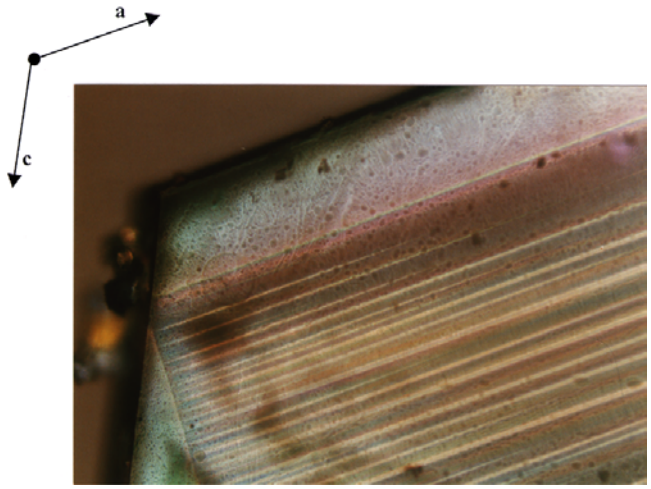

Figure 7. Ferroelastic domain structure in the a–c plane of PRCA at 145 K.
(This figure is in colour only in the electronic version)

(3) a small-angle libration of the pyrrolidinium cation,

(4) the rotations about the pseudo C_5' axis, which is perpendicular to the pyrrolidinium ring,

(5) isotropic rotation and cationic self-diffusion.

It is known that the cationic self-diffusion requires very high activation energies (more than 11 kcal mol^{-1}) [13]. The two different activation energy ranges found, 1.55–1.72 and 3.6–4.0 kcal mol^{-1}, we propose to assign to a small-angle libration and to a change in the conformation between twisted and envelope forms for pyrrolidinium cations, respectively.

No ionic plastic phase has been reached even at 410 K. Our studies lead to an important conclusion that the ionic plastic phases are rather typical for simple salts such as CsCl type [13, 15–17]. In the case of ionic salts, which are characterized by polymeric anionic structure, for example chloroantimonates (V), the ionic plastic phases are not expected to appear even at high temperatures.

The presented NMR results are the first attempt at the interpretation of all possible motional states of the pyrolidinium cations in a broad temperature range (27–410 K).

3.5. Optical observations

The optical observations of PRCA in the (a–c) plane were carried out by means of the polarizing microscope. Below the transition temperature $T = 152$ K one can observe platelike ferroelastic domains with walls parallel to the (010) planes (see figure 7). Further cooling of the sample showed that the domains disappear at 135 K. This PT is accompanied by a phase front which moves along the a axis. Such a behaviour confirms the first-order nature of the PT at 135 K. The appearance of the domains over the intermediate phase (152–135 K) is perfectly reversible if the 105 K PT is not crossed (see also figure 2, scans 1 and 2). The domain structure was only observed for very high-quality and very thin single crystals with the a–c plate.

3.6. Mechanism of the phase transitions in PRCA

It is instructive to compare the model of the pyrrolidinium cation disorder in PRCA with those encountered in numerous ionic salts containing the same organic cations. For the first example, pyrrolidinium hydrogen *bis*(*p*-methylbenzoate), the cations are disordered around a twofold axis [18]; however, this is not so in the case of PRCA. In $(C_4H_8NH_2)CuCl_3$ one of the carbon atoms opposite the N one of the ring has large displacement amplitude perpendicular to the plane of the ring. In spite of the fact that the disorder of the cation was evidenced, the position of this C atom could not be split [19]. Quite a similar situation was found in the case of a *bis*(pyrrolidinium) hexachlorometallate, $(C_4H_8NH_2)_2MCl_6$ (M = Sn, Te, Pt) [20]. A carbon atom C(2) opposite the N one was found to have two positions with equal occupancy. The C(3) atom of this ring showing strong anisotropic displacement was not separated. The semi-empirical MO calculations revealed two stable conformations; the twisted (C_2) and the envelope (C_s). The PT in $(C_4H_8NH_2)_2PtCl_6$ at 134 K accompanied by the entropy change of 7.5 J K^{-1} mol^{-1} is considered to be triggered by the configurational change in the cation ring. The two last presented models resemble to a great extent the situation found for the title crystal in the RT phase, for which two disordered cations (N(1) and N(6)) were found. It should be underlined that only the cation N(1) is characterized by especially large disorder. It is clear that the freezing of disorder of pyrrolidinium rings in PRCA has to take place between RT and 105 K. In our opinion the PT at 152 K is of 'displacive' type. Since 152 K PT is not visible in the ^{1}H NMR and dielectric studies, this excludes the organic cation contribution to the mechanism of this transition. The subsequent PT of first-order type at 135 K (on cooling) seems to have a similar character. The minor contribution of the cations to the mechanism of the 135 K PT was evidenced from the NMR studies. However, it is beyond doubt that the transition at 105 K is governed by the configurational order–disorder of the pyrrolidinium ring (or freezing of disorder of the C(3) atoms) and makes the most dominant contribution to the transition entropy ($\Delta S_{tr} = R \ln 3.4$).

The 374/351 K PT is clearly visible in the ^{1}H NMR and dielectric measurements. A distinct jump in the ε'_b value accompanying this PT may be interpreted as a releasing of motion of the dipolar groups in the crystal. The onset of a rapid reorientation of dipolar groups, such as pyrrolidinium rings, has to lead to an important change in the resultant dipole moment of the unit cell. It should be noticed that all pyrrolidinium cation rings are placed nearly parallel to the *a*–*b* plane (see figure 1). The releasing of the rotational motion of the cations may be visible as an important increase in the ε value above 374 K, along the *a* or *b* axis. This is actually observed in our dielectric measurements along the *b* axis.

In the RT phase of PRCA the disorder of the pyrrolidinium cations is connected with the shift of some carbon atoms perpendicular to the ring of cations which are placed in the *a*–*b* plane. Such a type of motion does not seem to lead to an important change in the resultant dipole moment of the unit cell (or electric permittivity) along the *c* axis. Furthermore, these changes for the *a* and *b* directions should be hardly visible. In our dielectric experiment carried out along the *b* axis the electric anomalies around 135 and 105 K are really small, which confirms our suggestions.

It is interesting to compare the ferroelastic PTs in all chloroantimonate (V) salts forming two classes, i.e. $RSbCl_6$ and $RSbCl_6{\cdot}RCl$. For the latter type of crystal only two salts have been studied up to now: $(C_4H_8NH_2)SbCl_6{\cdot}(C_4H_8NH_2)Cl$ and $(C_5H_{10}NH_2)SbCl_6{\cdot}(C_5H_{10}NH_2)Cl$ (PCAPC). PCAPC is characterized by crystal structure analogous to that of the PRCA crystal. In spite of this similarity the sequence of the PTs is quite different. PCAPC undergoes only one PT at 202 K of para–ferroelastic type ($Pccn \rightarrow P2_1/c$). The mechanism of this

PT is partially connected with disordering of the piperidinium cations. In the paraelastic phase there is present a puckering motion between two chair conformations of the cations yielding to a low-frequency dielectric dispersion process. The common feature of PRCA and PCAPC analogues is the presence of the para–ferroelastic PT of second-order type in the low-temperature region. It seems that in both crystals, apart from the cation contribution, the crucial role in the mechanism of the para–ferroelastic PT may be played by the changes in the hydrogen bond system formed between the N atoms and isolated Cl^- ions in the lattice. The N–H$\cdots$Cl interactions may lead to an important distortion of the crystal lattice and the appearance of the spontaneous deformation (ferroelasticity) in the $RSbCl_6{\cdot}RCl$-type crystals.

In the case of the $RSbCl_6$ type of crystal (where R = $P(CH_3)_4^+$, $C(NH_2)_3^+$, $(C_2H_5)_3NH^+$, $C_5H_{10}NH_2^+$) the para–ferroelastic PTs take place in the high-temperature range (from 336 to 369 K). In such a system the N–H$\cdots$Cl bonds formed between cations and Cl atoms belonging to the $SbCl_6$ units are distinctly weaker than those found in $RSbCl_6{\cdot}RCl$-type crystals. One can conclude that both the mechanism and sequence of the PTs in chloroantimonate (V) salts are distinctly determined by the N–H$\cdots$Cl hydrogen bond system.

4. Conclusions

(1) The structure of PRCA consists of isolated $SbCl_6^-$ anions and $(C_4H_8NH_2)^+$ cations connected by weak N–H$\cdots$Cl hydrogen bonds to isolated Cl^- ions. PRCA undergoes a complex sequence of PTs: at 351/374 K of first-order type (cooling/heating), 356 K (recorded on heating) and 152 K of second order and at 135/145 K and 105/134 K of first-order type. The ^{1}H NMR and dielectric studies evidence the pyrrolidinium cations' contribution to the mechanism of the PT at 105 and 374 K. To our knowledge the present ^{1}H NMR results are the first report on the molecular dynamics of the pyrrolidinium cations in the relatively wide temperature range 37–410 K.

(2) The optical observations clearly show that PRCA possesses ferroelastic properties between 152 and 135 K.

(3) Comparing the properties of alkylammonium chloroantimonate (V) salts studied up to now with those found for $(C_4H_8NH_2)SbCl_6{\cdot}(C_4H_8NH_2)Cl$, one can state that the type of crystal structure and the connected layout of hydrogen bonds for two different subclasses, $RSbCl_6$ and $RSbCl_6{\cdot}RCl$, determine both the sequence of the PTs and the temperature range of presence of the ferroic properties.

(4) The ferroic (ferroelastic) properties in all alkylammonium chloroantimonates (V) are strictly connected to the deformation of the hydrogen bond system with temperature. Most of the para–ferroelastic-type PTs revealed continuous character. The 'displacive' mechanism of these transitions is a result of coupling between the hydrogen bonding scheme and the anionic sublattice.

(5) The studies of the title crystal allow a better understanding of the nature and the mechanism of induction of ferroic properties in alkylammonium chloroantimonate (V) salts.

Acknowledgments

This work was supported by the Polish State Committee for Scientific Research (project register 3 TO9A 058 17) and partially (WM) in the frame of statue research of IMP PAS Poznań. The authors are indebted to Professor N Piślewski for helpful discussions and valuable comments.

References

[1] Ciąpała P, Jakubas R, Bator G, Pietraszko A and Kosturek B 1998 *J. Phys.: Condens. Matter* **10** 5439
[2] Jakubas R, Ciąpała P, Pietraszko A, Zaleski J and Kusz J 1998 *J. Phys. Chem. Solids* **59** 1309
[3] Bednarska-Bolek B, Ciunik Z, Jakubas R, Bator G and Ciąpała P 2002 *J. Phys. Chem. Solids* **63** 507
[4] Pietraszko A, Bednarska-Bolek B, Jakubas R and Zieliński P 2001 *J. Phys.: Condens. Matter* **13** 6471
[5] Bednarska-Bolek B, Pietraszko A, Jakubas R, Bator G and Kosturek B 2000 *J. Phys.: Condens. Matter* **12** 1143
[6] KUMA Diffraction Software 1998 versions 8.1.0, 8.1.1 (Wrocław: KUMA Diffraction)
[7] Sheldrick G M 1997 *SHELX-97. Program for Solution and Refinement of Crystal Structure* University of Göttingen
[8] Sheldrick G M 1990 *SHELXTL* (Madison, WI: Siemens Analytical X-Ray Instruments)
[9] Zaleski J and Pietraszko A 1996 *Acta Crystallogr.* B **52** 287
[10] Bujak M and Zaleski J 2001 *Cryst. Eng.* **4** 241
[11] van Vleck J H 1948 *Phys. Rev.* **74** 1168
[12] Powels J G and Gutowsky H S 1955 *J. Chem. Phys.* **23** 1692
[13] Ono H, Ishimaru S, Ikeda R and Ishida H 1999 *Bull. Chem. Soc. Japan* **72** 2049
[14] Bloembergen N, Purcell E M and Pound V 1948 *Phys. Rev.* **73** 679
[15] Ono H, Ishimaru S, Ikeda R and Ishida H 1997 *Chem. Phys. Lett.* **275** 485
[16] Ono H, Ishimaru S, Ikeda R and Ishida H 1998 *Ber. Bunsen-Ges. Phys. Chem.* **102** 650
[17] Ishida H, Ikeda R and Nakamura D 1987 *Bull. Chem. Soc. Japan* **60** 467
[18] Misaki S, Kashino S and Haisa M 1989 *Acta Crystallogr.* C **45** 917
[19] Wei M, Willet R D, Teske D, Subbaraman K and Drumheller J E 1996 *Inorg. Chem.* **35** 5781
[20] Ishida H, Furukawa Y, Sato S and Kashino S 2000 *J. Mol. Struct.* **524** 95